# Tracking Experiments with ChevBot: A Laser-Actuated Stick-Slip Microrobot

Ruoshi Zhang, Andriy Sherehiy, Danming Wei, Zhong Yang, M. Nasser Saadatzi, Dan O. Popa

Abstract—The idea of utilizing laser energy to actuate and control microrobots has been envisioned for several past decades and has already been demonstrated in liquid environments. ChevBot is a novel microrobot driven by laser energy that targets operation in dry environments, such as in a future microfactory. The microrobot operates using stick-slip locomotion by converting opto-thermal energy from a focused laser source into mechanical energy using "chevron-style" actuators. ChevBot's body components are fabricated using Micro-Electro-Mechanical-System (MEMS) technology and completed using a microassembly process. In this paper, we present modeling and simulation results, validated by experimentation measuring the robot's locomotion performance under varying conditions. The microrobot is automatically tracked through a visual servoing scheme using a microscope, a 3-DOF positioning system, and is powered by a 532nm 2W ND-YAG laser source. Experiments suggest that ChevBot velocities in excess of 100µm/s are achievable.

# Keywords—Microrobot, Microassembly, Microfactory

#### I. INTRODUCTION

Several ambient fields have been studied over the last three decades to accomplish remote powering and control of microrobots. These fields include electrostatic, magnetic, electromagnetic, light, and ultrasonic vibration energy delivered to mobile agents with sizes below 1 mm. The Mobile Microrobotics Challenge [1] has emerged as a platform for testing these propulsion methods in a competition format. Among remote actuation methods, magnetic fields have traditionally been among the most widely employed [2-5]. For example, in their recent work, Giltinan et al. [6] demonstrated a microrobot operated in magnetic field that performed a pegin-hole insertion without feedback control.

Laser actuation of microrobots is a remote powering method that has limitations due to its directional nature and requires simultaneous tracking control with the microrobot in motion. The Robofly [7] is an example of the use of laser light as a source of energy to power the microrobot. Based on RoboBee [8], Robofly was able to take off by replacing the tethered power source with a 3mm by 3mm photovoltaic solar cell irradiated with laser light, which demonstrates the feasibility of satisfying the power budget requirement for this demanding application.

Utilizing laser as both power and control source is a novel idea and so far, realized on some uncommon types of microrobots. "The bubble microrobots" demonstrated by W. Hu et al. [9] is another successful example of using light energy to actuate a microrobot using thermal convection effects. In his work, a bubble microrobot was trapped in silicon oil, and by directing a laser beam into the liquid in close proximity to the bubble, the resulting temperature change induces surface

tension gradients and Marangoni effects, which drive the microrobot. Multiple examples of open-loop manipulation tasks achieved by the bubble microrobot was also demonstrated with different targets, materials, and velocities [10]. As the next step, the bubble microrobot system design was accomplished with closed-loop automated control [11]. Within certain conditions, using bubble as microrobot has unique advantages - it is simple, highly effective on micro-meter sized objects, cost-efficient, potentially non-intrusive, and bio-compatible. However, this type of microrobot can be formed only in certain types of liquids, hence its application is limited. Another wellstudied example of laser actuation for microrobots is optical trapping and tweezing. This method uses the pressure impingement effect of a laser beam onto micron-sized transparent objects, such as silica beads, or biological cells [12]. This actuation method can generate relatively modest pN level forces, and therefore it is also limited to operation in liquid environments.

In this paper, we present a novel microrobot – the ChevBot, powered by laser energy and intended for microfactory applications in dry environments. The ChevBot is fabricated using MEMS and microassembly, has a footprint of approximately 400  $\mu$ m  $\times$  700  $\mu$ m  $\times$  40  $\mu$ m, and is capable of fast gating speeds on a silicon surface. In our previous work [13], opto-thermal-dynamical models were introduced, which predicted the stick-and-slip motion as well as turning abilities of this robot. Recently, these models were experimentally validated with preliminary experiments [14]. The ChevBot locomotion is accomplished via a thermal actuator located at the center of its body frame, which converts pulsed light energy from laser spot to a fast-changing temperature-induced vibratory motion. Combined with "feet" and "dimples" in contact with the substrate, the actuator generates a stick and slip motion.

We used the insights gained during modeling, and experimentation in [13] [14] to propose a new ChevBot design with considerable improvements to its directional motion stability, and its future maneuverability and controllability. Furthermore, an automated laser-robot tracking system was designed and implemented using visual servoing in order to ensure continuous powered operation for the microrobot and record gating trajectories. Results indicate that the ChevBot generates straight trajectories with speeds excess of  $100\mu m/s$ .

This paper organized as follows: Section II describes considerations of the microrobot design; Section III discusses fabrication and assembly of the microrobot; Section IV describe the experimental hardware used for driving and metrology; Section V discusses experimental results for both tethered and untethered microrobot testing scenarios; Finally, Section VI

<sup>\*</sup>Authors are with the Next Generation Systems (NGS) Group, Department of Electrical and Computer Engineering, University of Louisville, KY, USA, 40245. Email {firstname.lastname@louisville.edu}.

concludes the paper and proposes future work.

## II. MICROROBOT DESIGN

ChevBot is an assembled MEMS microrobot from Silicon components and is driven by a collimated laser beam approximately 800  $\mu m$  in diameter (Fig. 1). In the design studied in this paper, ChevBot has four major parts: two "feet" extending from the body frame, forming a 135° angle; the thermal actuator and its shuttle "anchored" within the body frame, and a dimple attached to the assembly pad of the shuttle. The microrobot measures  $734\mu m$  in length and  $427\mu m$  in width, and with an assembled dimple, its height is approximately  $40\mu m$ . Each beam in the thermal actuator is  $5\mu m$  wide and they form an acute angle of approximately  $87^\circ$  with the body frame. Fig. 1 depicts a design with 6 pairs of chevron beams, each approximately  $5\mu m \times 200\mu m \times 200\mu m$  in size.

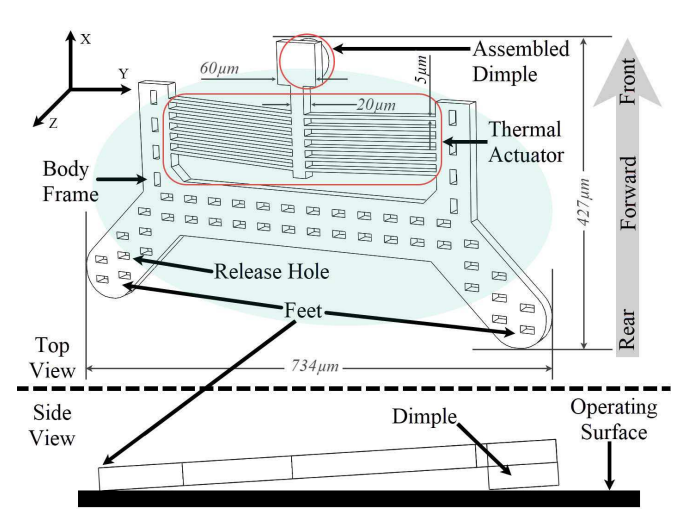


Fig. 1. 3-D drawing of ChevBot with critical dimensions. Consistent with locomotion direction, the assembled dimple is defined as the front of the robot, and the feet are defined as rear of the microrobot. The green ellipse represents the laser spot with large waist diameter  $w_{dmin} = 800 \mu m$  and small waist diameter  $w_{dmin} = 600 \mu m$ .

After the dimple is assembled, the ChevBot can lay on an operating surface at a small inclination angle, with the inner edge of the cylinder-shaped dimple and the feet as three contact points to the environment.

# A. Principle of Operation

A stick-and-slip model was adopted to describe and predict the motion of the microrobot [13] [14]. The power and control signal generating the gait is provided by a collimated laser beam that covers the entire body of ChevBot; meanwhile, the pulse laser beam can be operated under both burst and continuous mode to initiate actuation. Pulsed laser operation was chosen in order to induce cooling-heating cycles of the ChevBot's body, which in turn cause cyclical motion of the dimple, due to the thermal expansion effects. To sustain motion, the laser coverage of the microrobot needs to be maintained, e.g. the laser beam must follow the motion of the microrobot. During the laser-on cycle, the temperature of the microrobot body rapidly increases and activates the thermal actuator, which causes the dimple to stick to the substrate and the feet to slip toward the dimple. During laser-off, cooling cycle, the feet stick to the substrate and push the dimple forward to finish a full cycle of stick-and-slip motion, resulting a net forward displacement.

# B. Design Efforts Toward Straight Trajectory Locomotion

The control of the Chevbot's motion depends on its geometry. Therefore, design and relative location of the chevron actuator, dimple, and legs need to be considered to enable locomotion on a flat surface in a controlled way. It is not immediately clear how many feet or dimples must be located at the front or rear of the microrobot. Below we discuss why the choice of design in Fig. 1 is likely to result in locomotion along straight trajectories.

In a simplified general case, the microrobot contacts the operating surface through dimples and feet, represented by squares in Fig. 2. The circle represents the body/actuator of the microrobot, and the lines represent the "limbs" that connect the body with the feet. In a stick and slip gait, either the feet on the front or at the rear of the microrobot serve as the driver, while the other pair keeps balance, acting as a "supporter".

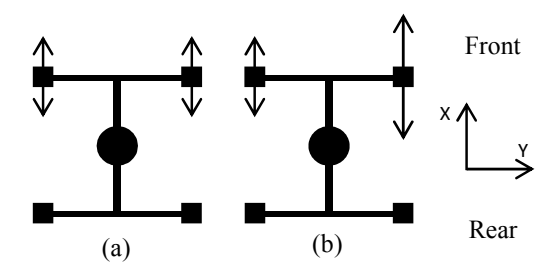


Fig. 2. Abstraction of the ChevBot design depicting the body (circle) and feet (square). The arrows indicate the reciprocating direction of the feet motion when actuating force is (a) balanced; (b) imbalanced.

In the above schematic, the driver feet reciprocate back and forth, and produce friction/stiction contact with the substrate to generate locomotion. The effect of driving force can be either pulling the microrobot forward to the X direction as shown in Fig. 2 (a) or pushing back towards -X direction as shown in Fig. 2 (b). While the first resulting motion is stable, the second motion is not, similarly to a front wheel/rear wheel automobile driving scenario. Furthermore, in practical scenarios, the feet experience imbalanced friction forces or net moments due to varying surface conditions and manufacturing imperfections, causing the microrobot to steer unpredictably.

Therefore, to improve the locomotion stability of the ChevBot compared to the design in [14] we want to ensure that the front feet pulls the microrobot forward, rather than push it backward. This was accomplished by reducing the two front feet to a single "dimple" location and orienting the chevron direction of the microactuator in the direction which causes desired forward locomotion, resulting in the ChevBot design shown in Fig. 1.

# III. FABRICATION AND ASSEMBLY

The ChevBot was fabricated from a Silicon wafer using a standard SOI process, and further assembled with a custom microassembly in our lab, as described in this section.

# A. Fabrication

The ChevBot was fabricated on a silicon on insulator (SOI) wafer with  $20\mu m$  device layer thickness using a Deep Reactive Ion Etching (DRIE) process. The microrobot layout, its dimple and other assembly components are depicted in the mask design

shown in Fig. 3.

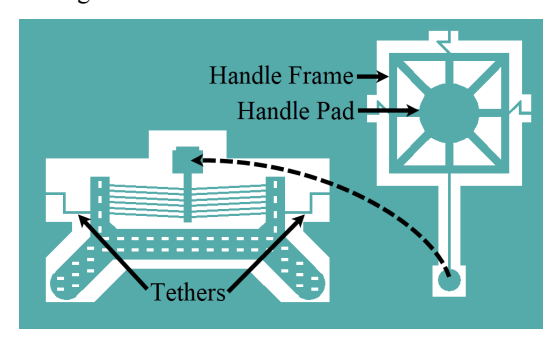


Fig. 3 Mask layout of ChevBot body and its dimple assembly.

First, the wafer was first cleaned using the RCA process to remove any potential organic, oxide and iconic contamination. Second, photolithography was performed by spun photoresist Shipley 1827 on the dried wafer surface, and soft baked on a hot plate. An UV exposure was performed to transfer the patterns on the mask onto the photoresist. Then, the photoresist was developed in the designated developer to finish photolithography. Third, after inspection of the photoresist under microscope, the wafer was placed on the hot plate again to hard bake, so that the photoresist was hardened and ready to serve as a masking layer for DRIE.

The subsequent etching process carved the body of the microrobot out of the device layer of the SOI wafer. Preliminary etching time was empirically estimated, depend on the overall etching area and the etching rate of the machine for a given recipe. After etching for 20 minutes, the sample was removed from the chamber and the actual etching rate was estimated by dividing the measured trench depth with time. The photoresist mask along with process byproducts were removed after a successful DRIE process by oxygen plasma clean in a March RIE machine.

Another layer of photoresist was spun before dicing the wafer, so that the particles created during dicing would not fall into DRIE trenches and block the motion of the microrobot. The spin rate of this step is slow and does not require very hard photoresist. Finally, release and drying were performed after dicing. Individual dies were merged in 49% HF acid for 10 minutes to release. After the 10 minutes period, all dies were removed from acid and rinse under deionized water in a plastic container to wash away HF acid. Drying was then automatically done using supercritical CO<sub>2</sub> in a Critical Point Dryer tool.

### B. Assembly

ChevBots were assembled by the custom NeXus microassembly station shown in Fig. 4. The NeXus consists of two motorized manipulators  $M_1$  and  $M_3$ , each targeting different set of manipulation tasks. The  $M_1$  manipulator holds the sample chuck, and contains two identical linear translation stages, stacked perpendicularly to each other at the bottom, and a rotation stage on top. The sample chuck is made of aluminum, with five vacuum-secured 1cm by 1cm die slots on top. Overall, the  $M_1$  manipulator fulfils X-Y- $\theta$  motion to the sample chuck. The  $M_3$  manipulator consists of a manual Z stage to adjust height, three motorized linear translational stages and one rotational stage stacked together to fulfil X-Y-Z- $\theta$  motion for the end-effector. The rotational stage is mounted vertically on the Z stage, with a 3D printed fixture and an adapter, and a

vacuum tip end-effector installed horizontally. The dimple is picked up with a vacuum tip, moved to the desired location, and bonded to the assembly pad using UV epoxy.

Assembly of the ChevBot aims to bond the dimple onto the front foot and flip the microrobot body so it forms a three-point contact with the operating surface. To simplify the assembly process, the ChevBot body and the dimple assembly were placed on the same die; before picking up the dimple, a small amount of UV adhesive (BONDIC® L4G 3V5, Aurora, ON, Canada) was dissipated near the assembly site; then, with a probe tip, we broke the tethers that hold the dimple assembly, and the vacuum tip end-effector was aligned with the handle pad at the center. With the help of the handle frame, the operator slightly dipped the dimple in the pool of UV adhesive, then placed the dimple onto the assembly pad. Finally, a UV torch light was used to cure the adhesive in place.

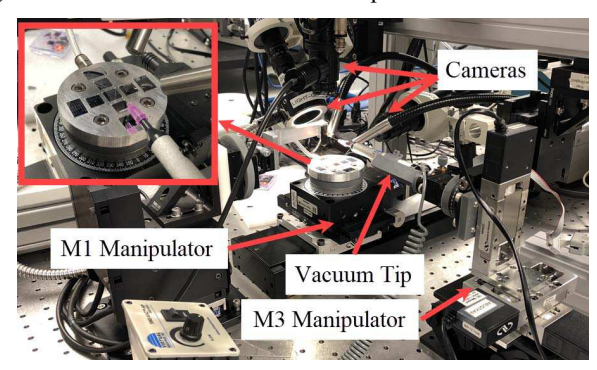


Fig. 4 The NeXus microassembly station used to assemble ChevBots.

# IV. EXPERIMENTAL POWER AND TRACKING SYSTEM

In order to power and track ChevBot, we configured a custom experimental system as a combination of two subsystems: an optical system for laser delivery and an automated visual tracking stage system to compensate microrobot's motion, so that ChevBot continuously stays under the laser beam. This system was used for two different experiments, one involving tethered microrobots to the substrate die, and another to study the motion of untethered microrobots on operating surface. In the case of the tethered ChevBot, only motion of the thermal actuator was measured. In the untethered case, the goal was to initiate and record stick and slip motion of the whole microrobot on a silicon substrate.

#### A. Optical System for Laser Delivery

Laser irradiation tests with ChevBot were conducted using an experimental setup depicted in Fig. 5. The main components of the optical testing system include:

- Explorer One Nd:YAG laser from Spectra-Physics, with 532nm wavelength, 2W Maximum power, 0.5-60 kHz repetition rate and 10 to 40ns pulse time width.
- A system of lenses, neutral density (ND) filters, beam splitters and mirrors to deliver the laser beam to the microrobot.
- Four Newport X-Y positioning stages of 423 and 443 series, with two actuated by linear actuator TRA25CC and two controlled manually. They stack perpendicular to each other, while sample chuck was fixed on top.
- Tube lens, illuminator, beam splitter, National Instruments smart camera ISC-1772C for automated tracking and Pixelink CMOS camera for visualization.

 A range sensor, LK-H008 from Keyence, to measure the displacement of the thermal actuator in tethered experiments.

During the experiments, the laser beam was passed through the neutral density filter and system of the lenses, toward the set of the adjustable mirrors, which directs laser light onto the ChevBot on the sample chuck. The last mirror is placed at angle, so that incident laser beam is at 20° to 30° angle to the normal of the arena's surface. As a result, the laser spot has an elliptical shape on the sample surface with a large waist diameter w<sub>dmax</sub>=800μm and small waist diameter w<sub>dmin</sub>=600μm. The laser spot and ChevBot are aligned with help of the Pixelink CMOS camera, which is coupled with the NI smart camera by a beam splitter, so that both share the same field of view of the sample on the stage chuck. Both cameras and beam splitter are attached to the tube lens that is placed above the sample chuck. The laser module can be operated under either continuous or burst mode. Continuous mode generates a series of pulses, while under burst mode, user can specify the number of pulses within a burst and delay between each burst. For both cases, repetition rate of the fundamental pulses and diode current are adjustable. Thus, the power of the laser is affected by diode current and number of pulses within each burst.

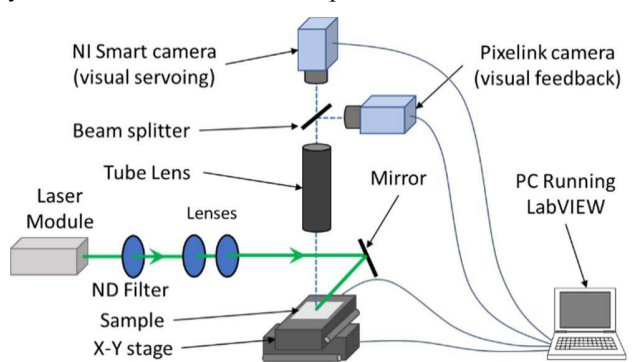


Fig. 5 Schematic of laser delivery and vision acquisition system.

## B. Vision Acquisition and Automated Motion Tracking

For untethered microrobot experiments, the laser beam was focused onto the ChevBot with sufficient power to initiates gating motion, which in turn causes the robot to escape from the laser beam waist. At that point the microrobot loses power, the laser beam needs to be repositioned to track the motion of the robot. Typical laser trackers will reposition the beam either through a series of movable mirrors, or through physical repositioning of the laser beam source. In a novel twist, we keep the laser beam position fixed, but we reposition the robot to the laser spot using a visual servoing scheme implemented by camera feedback and described in Fig 6.

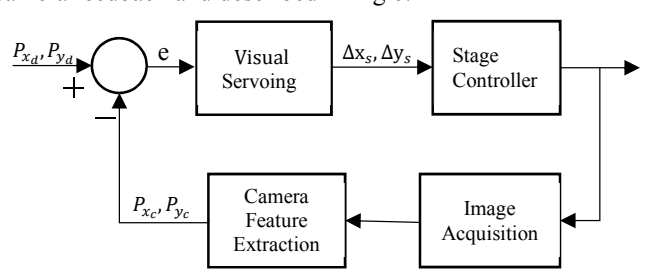


Fig. 6 Control scheme of the combined laser-beam robot motion.

Our vision feedback scheme is based on the NI smart

camera which contains a color sensor with resolution of 640 by 480 and an Intel® processor. The smart camera processes images and extracts the pixel location of the microrobot with the pattern matching feature, then the pixel location is sent to a laptop PC that runs LabVIEW® to drive the X-Y stages to maintain the microrobot under the laser spot.

An Image Jacobian was identified for visual servoing, which bridges the mapping between sampled pixel position to the X-Y stage's displacement. The Jacobian was estimated with seven randomly picked locations under the observation of the camera. If  $P_x$  and  $P_y$  are the position of the centroid of the microrobot feature observed under the camera, the image Jacobian has 4 entries that can be estimated, and connects the pixel variations to the stage position variation according to:

$$\begin{bmatrix} \Delta P_X \\ \Delta P_Y \end{bmatrix} = J \begin{bmatrix} \Delta X \\ \Lambda Y \end{bmatrix},\tag{1}$$

$$J = \begin{bmatrix} J_{11} & J_{12} \\ J_{21} & J_{22} \end{bmatrix}, \tag{2}$$

in which J is the 2x2 image Jacobian,  $\Delta P$  is the difference of current position to previous position in pixels, and  $\Delta X$  and  $\Delta Y$  are variations in the X-Y stage coordinates expressed in encoder counts.

In order to maintain the ChevBot at the center of the camera image, where the laser has been focused, the visual servoing feedback provides current pixel location of the ChevBot  $(P_{x_c}, P_{y_c})$ , then compared with the desired pixel location  $(P_{x_d}, P_{y_d})$  to generate an error term used to drive the stages to a new location using a proportional controller:

$$\begin{bmatrix} X_{new} - X_c \\ Y_{new} - Y_c \end{bmatrix} = \Delta s J^{-1} \begin{bmatrix} P_{X_d} - P_{X_c} \\ P_{Y_d} - P_{Y_c} \end{bmatrix},$$
 (3)

where  $\Delta s$  is a parameter step-size of 0.5 and  $J^{-1} = \begin{bmatrix} -0.0089 & -0.0007 \\ -0.0011 & -0.0076 \end{bmatrix}$ , as identified through calibration.

## V. EXPERIMENTAL RESULTS AND DISCUSSION

We conducted several experiments to confirm our ChevBot design choices and measure the microrobot resulting displacements and trajectories under laser power.

# A. Experiments with tethered robots for model identification

In this experiment, the robot actuator displacement was measured while the robot was tethered to the SOI device layer, which characterizes the actuator displacement and identifies components of a mass-spring-damper model. The repetition rate of the laser was set to 1700Hz for maximum actuator displacement based on results from [14], and the laser diode current was considered as input to system identification. The system's output was the displacement of the thermal actuator, measured by the Keyence® displacement sensor.

A testing die was prepared such that many tethered ChevBots were located at the edge, and therefore the sensor laser beam can be reflected from the side wall of the thermal actuator to acquire the dynamic measurement. During this experiment, the laser module works under continuous mode and a pseudo random binary sequence (PRBS) was generated to

toggle the laser diode, hence apply laser power to the microrobot, while the displacement sensor collected data at a sampling rate of 10kHz. A LabVIEW® program was designed to collaborate the sensor and the laser module. Collected data is depicted in Fig. 7 and reveals that chevron actuator displacements of 300nm are achievable with this level of power output, which also suggests that the minimum step size of the microrobot falls in this range. If the laser power is reduced, the achievable minimum microrobot step sizes can also decrease.

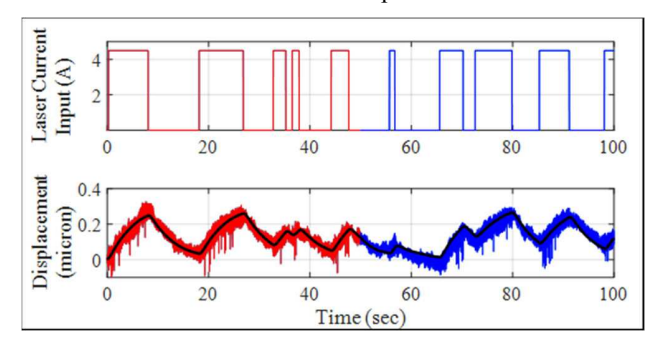


Fig. 7 Laser power stimulus as input (top) and ChevBot thermal actuator displacement as output (bottom). The red and blue graphs represent the estimation and validation datasets, respectively. The black fitting line is the output of identified model to the PRBS input.

In the tethered configuration, the ChevBot's frame is stationary, and the actuator and dimple can be modeled as a mass-spring-damper system. Therefore, by taking the thermal aspect of the system's behavior into account, a third-order transfer function is expected to properly explain the overall dynamic behavior of the system from the laser actuation to the resulted displacement. Using MATLAB's system identification toolbox, a third-order transfer function was fitted to the estimation dataset. The fitness score of the estimation and validation datasets were 0.66 and 0.62, respectively, and the resulting transfer function obtained was:

$$H(s) = \frac{0.195}{(s+0.196)(s^2+5.096s+13.95)}$$
(4)

However, in order to check for model overfit, another system identification was performed fitting a first-order transfer function into the estimation dataset, resulting in a similar fit via:

$$H(s) = \frac{0.014}{(s+0.196)} \tag{5}$$

The fitness score of the estimation and validation datasets were 0.65 and 0.60, respectively. As a result, we concluded that our fitted first order model captures the thermal behavior of the chevron actuator, and that the mechanical modes of the system are not excited by this laser pulse frequency. Next, utilizing the stick-and-slip model introduced in [14], we simulated the untethered motion of the ChevBot by introducing a chevron actuator force obtained from laser power filtered through H(s). The microrobot mechanical system was represented by a double mass-spring-damper with values obtained from the microrobot geometry, in particular, the spring constant K=624N/m and masses  $M_{\text{foot}}=1.1\mu g$ ,  $M_{\text{body}}=3.3\mu g$ . Although the surface condition represented by stiction and friction will vary, a dynamic model of the ChevBot using a Coulomb static and dynamic friction model with coefficients  $\mu_s=0.4$ , and  $\mu_d=0.33$ predicts that locomotion velocities of 53 µm/s can be expected.

## B. Experiments with mobile ChevBots

In the second series of experiments, assembled ChevBots were actuated on a silicon substrate by burst mode laser power. Each experiment took a few minutes, until the microrobot reaches the edge of the arena or its motion was blocked by dust particles. In general, experiments confirm that the ChevBot microrobot generates a straight trajectory heading towards its front direction, as shown in Fig. 8 with all trajectories beginning from the origin. Five sets of experiments were conducted to determine the effect of different laser parameters and surface condition on speed (Table I). The trajectory plots of the ChevBot were recorded while the microrobot was tracked using both the X and Y encoder readings of the stages, and the servoing camera image coordinates.

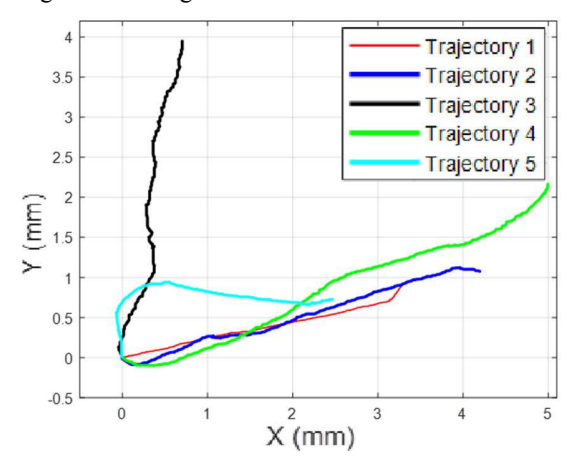


Fig. 8 ChevBot's trajectory from 5 different experiments, measured within a time span of 90 seconds.

As most of the trajectories illustrate, Chevbot does not follow ideally straight path, experiencing sudden turns and stops. Such behavior can be caused by variations in surface conditions suggesting that the microrobot encounters dust specks or stiction patches on the substrate. It can also be caused by non-uniform irradiation of the Chevbot's body due to the elliptical shape of the laser beam's spot, as well as its position relative to the microrobot. Clarifying the importance of these effects needs more study in our future work.

As summarized in Table I, the robot velocity measured from the trajectory data, is reported as an average along with standard deviation ( $\Sigma$ ). The relatively large standard deviation suggest that measuring velocity using stage encoders is inaccurate. As a result, velocity was also measured from video recording of the experiment for a more accurate estimation, generally in the range of 20 to 110  $\mu$ m/s. The velocity of the microrobot and amount of energy it receives show a positive correlation, e.g. velocity increases when more power is delivered.

TABLE I. UNTETHERED LOCOMOTION MEASUREMENT RESULTS

Test	Pulses Per Burst	Burst Delay	Avg. Power	Stage Velocity	Σ	Measured Speed
1	30	200ms	388~454mW	39.1μm/s	26.1	21.8µm/s
2	40	200ms	388~454mW	23.6μm/s	10.6	32.2μm/s
3	40	100ms	410~468mW	51.2μm/s	36.7	90.6μm/s
4	50	100ms	432~490mW	65.4µm/s	24.0	83.4µm/s
5	50	50ms	440~504mW	90.3μm/s	40.4	109.0μm/s

In addition, the visual servoing error plot during the tracking experiments shown in Fig. 9 indicates that the deviation of the

robot away from the laser center is smaller than 30  $\mu$ m, thus guaranteeing that the robot is always powered within the waist beam of the laser. Finally, Fig. 10 shows four snapshots from one of the video recording of our experiment, in which the ChevBot successfully navigates over a dust speck, with a measured velocity of 55.9 $\mu$ m/s, very similar to the simulation prediction.

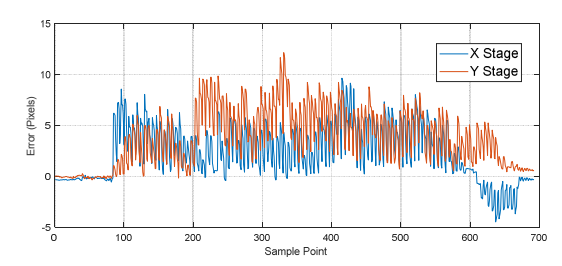


Fig. 9 Visual servoing tracking error of a typical trajectory in pixels. Each pixel is approximately 2 μm.

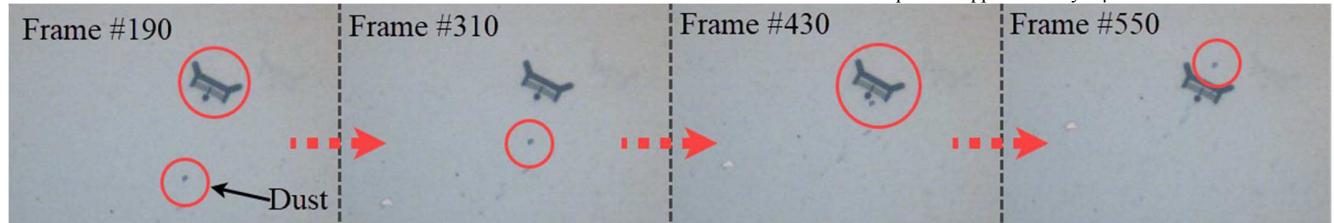


Fig. 10 ChevBot's trajectory during one experiment, with a measured velocity of 55.9 µm/s.

#### VI. CONCLUSION AND FUTURE WORK

In this paper, we propose and experimentally validate a laser-actuated ChevBot microrobot design that can achieve fairly straight, uncontrolled velocities on a dry silicon environment. Using a custom-configured optical delivery and tracking experimental system, we collected experimental data of operation for both tethered and untethered microrobots. Results obtained in tethered operation can be utilized to fine tune the parameters of an opto-thermo-mechanical model for ChevBots, and thus use the models to improve future microrobot performance. By using a visual servoing tracking scheme, untethered microrobots were continuously powered to characterize their operation on a silicon substrate. The experiment confirms the pulsed laser signal is responsible for the gaiting motion of the ChevBot. Furthermore, the results suggest that velocities in excess of 100 µm/s can be obtained, and that the motion characteristics are influenced by substrate condition. The experimental results suggest that ChevBot can be used as a micro or nano scale positioner in microfactory applications.

In future work, we will conduct a more comprehensive studies of the microrobot motion under various laser input, and surface characteristic conditions. The minimum and maximum step size of ChevBot will also be examined under high speed camera. Finally, we will work on implementing closed loop controllers to steer (rotate, translate) the robot along controlled trajectories. Control over the robot trajectory can be accomplished by designing differential thermal responses in its feet and dimple, by changing the frequency of the laser, and by controlling the relative location the laser beam and microrobot.

# ACKNOWLEDGMENT

This work was supported by NSF Grants #CMMI 1734383 and #MRI 1828355. We wish to thank the Micro Nano Technology Center staff at University of Louisville for help with cleanroom fabrication.

#### REFERENCES

[1] "Mobile Microrobotics Challenge," IEEE Robotics and Automation Society, [Online]. Available:

- https://sites.google.com/site/mobilemicrorboticschallenge/. [Accessed 18 2 2018].
- [2] E. Diller, S. Floyd, C. Pawashe and M. Sitti, "Control of Multiple Heterogeneous Magnetic Microrobots in Two Dimensions on Nonspecialized Surfaces," IEEE Transactions on Robotics, vol. 28, no. 1, pp. 172-182, 2012.
- [3] P. Ryan and E. Diller, "Magnetic Actuation for Full Dexterity Microrobotic Control Using Rotating Permanent Magnets," IEEE Transactions on Robotics, vol. 33, no. 6, pp. 1398-1409, 2017.
- [4] M. P. Kummer, J. J. Abbott, B. E. Kratochvil, R. Borer, A. Sengul and B. J. Nelson, "OctoMag: An Electromagnetic System for 5-DOF Wireless Micromanipulation," IEEE Transactions on Robotics, vol. 26, no. 6, pp. 1006-1017, 2010.
- [5] E. E. Hunter, E. B. Steager, A. Hsu, A. Wong-Foy, R. Pelrine and V. Kumar, "Nanoliter Fluid Handling for Microbiology Via Levitated Magnetic Microrobots," IEEE Robotics and Automation Letters, vol. 4, no. 2, pp. 997-1004, 2019.
- [6] J. Giltinan and M. Sitti, "Simultaneous Six-Degree-of-Freedom Control of a Single-Body Magnetic Microrobot," IEEE Robotics and Automation Letters, vol. 4, no. 2, pp. 508-514, 2019.
- [7] J. James, V. Iyer, Y. Chukewad, S. Gollakota and S. B. Fuller, "Liftoff of a 190 mg Laser-Powered Aerial Vehicle: The Lightest Wireless Robot to Fly," in 2018 IEEE International Conference on Robotics and Automation (ICRA), Brisbane, Australia, May 21-25, 2018.
- [8] K. Y. Ma, P. Chirarattananon, S. B. Fuller and R. J. Wood, "Controlled Flight of a Biologically Inspired, Insect-Scale Robot," Science, vol. 340, no. 6132, pp. 603-607, 2013.
- [9] W. Hu, K. S. Ishii and A. T. Ohta, "Micro-assembly using optically controlled bubbles," in 16th International Conference on Optical MEMS and Nanophotonics, Istanbul, Turkey, 8-11 Aug. 2011.
- [10] K. S. Ishii, W. Hu and A. T. Ohta, "Cooperative micromanipulation using optically controlled bubble microrobots," in IEEE International Conference on Robotics and Automation, Saint Paul, MN, USA, 2012.
- [11] N. Takahashi, Z. Wang, M. A. Rahman, J. Cheng and A. T. Ohta, "Automated micro-object caging using bubble microrobots," in 2016 IEEE 11th Annual International Conference on Nano/Micro Engineered and Molecular Systems (NEMS), Sendai, Japan, April 2016.
- [12] H. Chen, C. Wang, X. Li and D. Sun, "Transportation of Multiple Biological Cells Through Saturation-Controlled Optical Tweezers in Crowded Microenvironments," IEEE/ASME Transactions on Mechatronics, vol. 21, no. 2, pp. 888-899, 2016.
- [13] M. R. Pac and D. O. Popa, "3-DOF Untethered Microrobot Powered by a Single Laser Beam Based on Differential Thermal Dynamics," in 2011 IEEE International Conference on Robotics and Automation, Shanghai, China, 9-13 May 2011.
- [14] R. Zhang, A. Sherehiy, Z. Yang, D. Wei, C. K. Harnett and D. O. Popa, "ChevBot – An Untethered Microrobot Powered by Laser for Microfactory Applications," in 2019 International Conference on Robotics and Automation, Montreal, Canada, 2019.